The Performance of Rotating Membrane Emulsification in the Presence of Baffles

Bruno, Chloe; Tripodi, Ernesto; Werner, Dominik; Windows-yule, Christopher; Spyropoulos, Fotios

DOI:
10.1016/j.ces.2023.119476

Document Version
Publisher's PDF, also known as Version of record

Citation for published version (Harvard):
Bruno, C, Tripodi, E, Werner, D, Windows-yule, C & Spyropoulos, F 2024, 'The Performance of Rotating Membrane Emulsification in the Presence of Baffles: Insights from Flux Experiments, Microstructural Analysis, and Positron Emission Particle Tracking', *Chemical Engineering Science*, vol. 284, 119476. https://doi.org/10.1016/j.ces.2023.119476

Chemical Engineering Science 284 (2024) 119476

Contents lists available at ScienceDirect

Chemical Engineering Science

journal homepage: www.elsevier.com/locate/ces

The performance of rotating membrane emulsification in the presence of baffles: Insights from flux experiments, microstructural analysis, and positron emission particle tracking ☆

Chloe Huckvale Bruno *, Ernesto Tripodi, Dominik Werner, Christopher Windows-Yule, Fotis Spyropoulos

School of Chemical Engineering, University of Birmingham, Edgbaston, Birmingham, B15 2TT, United Kingdom

ARTICLE INFO

Keywords:
Emulsification
Rotating membrane emulsification
Baffles
Positron Emission Particle Tracking (PEPT)
Emulsion throughput

ABSTRACT

Rotating Membrane Emulsification (RME) is a bottom-up emulsification technique developed to circumvent the significant energy requirements of conventional methods; however, its implementation has been hindered by low emulsion throughputs. This work presents a novel baffled-RME setup and investigates the potential improvement to emulsion throughput and droplet microstructure, whilst employing both surface-active and Pickering particle emulsifiers to assess whether any advantages are emulsifier-specific. Overall, baffle addition improves emulsion throughputs, however the droplet microstructure was positively influenced only when using surfactant-based emulsifiers. Positron Emission Particle Tracking (PEPT) was utilised to demonstrate that these advantages result from improved hydrodynamic conditions instigated by the break-up of streamlines, inducing higher turbulence near the membrane surface, and by increasing the transmembrane pressure drop and drag force through flow restrictions. Overall, by detailing the first baffled-RME setup and first application PEPT analysis to such equipment, this work lays the foundation for further optimisation of bottom-up emulsification approaches.

1. Introduction

The formation of liquid-liquid emulsions remains a key processing step in the production of a large number and variety of products in the food industry, imparting vital characteristics for consumer acceptance such as texture, mouthfeel, flavour enhancement, and appearance (Fellows, 2000; Tan and McClements, 2021). However, conventional emulsification equipment often relies on high-energy methods employing a top-down approach to achieve the desired average dispersed phase droplet size, requiring a large amount of energy to achieve product specifications and having low energy efficiency due to constant coalescence and break-up of emulsion droplets (Tripodi et al., 2020). Conversely, low-energy emulsification methods employ a drop-by-drop, bottom-up approach, resulting in several significant advantages as compared to their high-energy counterparts. These include an increased overall energy efficiency, a large extent of droplet size monodispersity, and reduced shear allowing the processing of more delicate components (Lepercq-Bost et al., 2008). One such method is Membrane Emulsification (ME), first introduced by Nakashima et al. in 1991 as a novel process capable of producing monodisperse emulsions with span values less than 0.5 (Nakashima et al., 1991). The principle of ME involves passing the dispersed phase through a membrane of defined pore size to form small uniform droplets, which are then broken off at the membrane surface and immersed in the continuous phase (Holdich et al., 2020). The process has evolved to consist of various possible membrane and dispersed/continuous phase arrangements such as dead-end, cross-flow, and rotating membrane emulsification, differing mainly in the mechanism by which droplets are detached from the membrane surface (Piacentini, 2015). Rotating Membrane Emulsification (RME) in particular has received increased interest in recent years due to its numerous advantages over other ME systems. This includes the use of shear via membrane rotation to facilitate earlier droplet detachment, whilst avoiding excessive droplet breakage as well as increased energy demand and associated running costs due to pump circulation, as is

☆ The work presented here was supported through funding by the Royal Society of Chemistry (U21-1821928367) and the University of Birmingham's Engineering and Physical Sciences Research Council (EPSRC) Impact Acceleration Account 2017-22 (IAA:EP/R5 11651/1).

* Corresponding author.
E-mail address: CXB1036@student.bham.ac.uk (C.H. Bruno).

https://doi.org/10.1016/j.ces.2023.119476
Received 2 July 2023; Received in revised form 8 October 2023; Accepted 4 November 2023
Available online 10 November 2023

often the case in cross-flow ME (XME) (Ekanem et al., 2022). This makes it suitable for the production and processing of delicate materials and microstructures, such as double emulsions (Vladisavljević and Williams, 2006). In the RME process, a tubular membrane of selected material is rotated inside a process vessel containing the continuous phase. The dispersed phase is pushed through the membrane due to a pressure differential between the inner and outer membrane surface (the transmembrane pressure, TMP) such that droplets are formed and detach into the continuous phase (Spyropoulos et al., 2014a). Droplets are formed at the membrane surface via a number of driving forces, including drag, buoyancy, inertial, lift and static pressure forces (Spyropoulos et al., 2014b), and are allowed to accumulate in the process vessel until the desired dispersed phase concentration is achieved. Many previous studies have documented successful use of RME to produce both surfactant and Pickering emulsions. Vladisavljević and Williams (2006) demonstrated production of coarse oil-in-water (o/w) emulsions using a 100 μm pore size laser-drilled stainless-steel membrane, with droplet diameters in the range of 80-260 μm, and emphasised the importance of careful processing parameter and membrane materials selection to achieve the desired emulsion characteristics (Vladisavljević and Williams, 2006). Yuan et al. (2009) reviewed and demonstrated the importance of membrane composition and pore structure on emulsion microstructural properties and potential enhancement of throughput, employing a stainless-steel membrane to produce coarse droplets at high throughput by varying the membrane pore morphology (Yuan et al., 2009). A prevalent disadvantage of RME highlighted in these previous studies is the difficulty to achieve a high emulsion throughput, which serves as a major obstacle to large-scale industrial adoption (Güell et al., 2016). Many have suggested that this could be overcome by scaling the membrane surface area in accordance with the required throughput (Aryanti et al., 2009), by employing process parallelisation techniques, or by thermally altering the dispersed phase viscosity to improve flux (Spyropoulos et al., 2014b). However these strategies pose significant drawbacks in terms of cost effectiveness in the former two cases, especially considering the high cost of specialized and recently developed laser-drilled metallic membranes, desirable due to the delivered advantages of increased pore size control (Yuan et al., 2009; Hancocks et al., 2016). Thermal manipulation of dispersed phase viscosity may also be unfavourable, as this negates the advantage of a reduced shear treatment in RME, restricting the potential to process more delicate materials (Spyropoulos et al., 2014b). Alternative methods to increase throughput without significantly increasing relative unit cost or sacrificing emulsion quality have also been explored. Ekanem et al. (2022) demonstrated the use of an integrated XME and RME unit, attempting to merge the benefits of high-throughput XME and an enhanced control over microstructure from RME (Ekanem et al., 2022). However, this study assumes that the transmembrane throughput is constant with time, considering only the effect of crossflow throughput on emulsion droplet size. In fact, it is postulated and confirmed in the present study that at high throughput, the transmembrane flux in RME may deviate from theoretical prediction, possibly due to a build-up of droplets close to the membrane surface owing to highly laminar flow conditions in the process vessel. Baffles are a common tool used to enhance mixing and turbulence in process vessels, and hence may help to mitigate the time dependency of RME throughput. However, to confirm the theorised explanations for the time dependent RME flux and justify the use of baffles in the RME process, it would be useful to gain insight on the flow conditions inside the unbaffled and baffled vessel. Positron Emission Particle Tracking (PEPT) is a non-invasive imaging technique employing positron-emitting particles to track the Lagrangian trajectory of granular or fluid systems in four dimensions (temporal and spatial) (Windows-Yule et al., 2020, 2022a). The technique relies on the detection of 511 keV gamma rays, emitted at approximately back-to-back trajectories via the annihilation of a positron with an electron, using two position-sensitive detectors (Herald et al., 2022). This allows fluid flows in opaque systems, such as emulsions, to be mapped with high accuracy so long as suitably active particle tracers with similar density to the present media are used (Langford et al., 2016). Full details of the PEPT technique may be found in reference (Windows-Yule et al., 2022b). The technique has been demonstrated as a highly effective flow visualization tool for various mixing problems in a wide range of process equipment (Bakalis et al., 2006; Chiti et al., 2011; Fangary et al., 2000; Mihailova et al., 2015; Pérez-Mohedano et al., 2015; Sindall et al., 2017), and hence is used in this study to evaluate the effectiveness of adding baffles to the RME process vessel in an effort to improve mixing conditions and prevent droplet congregation, as well as to gain further insight into the hydrodynamic conditions present throughout the equipment for different processing parameters. Thus, the aim of this study is to evaluate the potential benefits imparted to the RME method through the use of baffles, in terms of both emulsion throughput and droplet microstructure. In addition, the study explores the role of emulsifier type (surfactant vs colloidal Pickering particle species) on the benefits of a baffled RME setup. The method of Positron Emission Particle Tracking is then employed to take a closer look at the fluid dynamic behaviour within RME equipment of different geometries and baffle configurations. This data is then used to elucidate the causes of the differences in transmembrane flux, droplet size, and droplet size distribution when comparing baffled and unbaffled vessels by giving insight on the mechanism by which baffles enable improved processing results. The present study is the first to propose and test this novel RME configuration, while the use of PEPT to probe ME processing has not been reported previously either.

Table 1
Process Parameter Levels Used in Experiments.

Parameters and Levels		
Transmembrane Pressure (bar)	Number of baffles	Vessel internal diameter (cm)
1	0	10
1.5	4	8
2	8	

2. Materials and methods

2.1. Materials

2.1.1. Flux experiments

Oil-in-water (O/W) emulsions of 10 wt.% commercially available sunflower oil were produced using the RME equipment detailed in section 2.2.1. Double distilled water from Milli-Q systems (Millipore, Watford, UK) was used for the continuous phase to produce all emulsions in the flux measurements. Two emulsifier systems were investigated, resulting in both surfactant and Pickering stabilized emulsions. Hence both Tween 20 (polyoxyethylene 20 sorbitan monolaurate, Sigma Aldrich) at 1 wt.% and Ludox SM colloidal silica provided in 30 wt.% aqueous suspension (Sigma Aldrich) at 3 wt.% were used to stabilize the O/W systems. The silica suspensions required further preparation before use to reduce the suspension pH to approximately 2 using 1M hydrochloric acid. This served to decrease surface charge and allow close packing of the silica particles at the emulsion droplet interface (Arkoumanis et al., 2019).

2.1.2. PEPT experiments

The PEPT experiments employed different process vessel fluids than described in section 2.1.1. This was due to the desire to dampen the noise obtained when using pure water systems, and to ensure suspension of the tracer in the process vessel throughout experimental runs. Hence a 70/30 wt.% glycerol/water solution was used, as this composition most closely replicated the density of the tracer. Glycerol was provided by Sigma Aldrich, whilst water was obtained from the lab sink. Tween 20 (polyoxyethylene 20 sorbitan monolaurate, Sigma Aldrich)

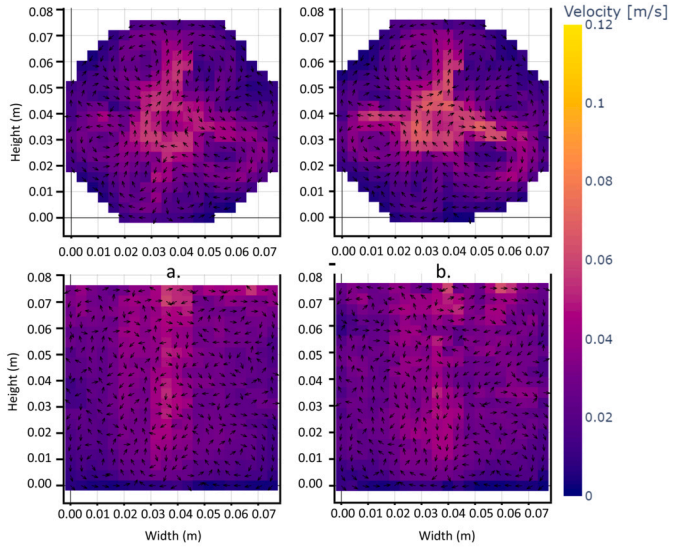

Fig. 1. Comparison of spatial velocity distributions obtained using 70/30 wt.% glycerol/water process fluid a) without, and b) with 10 wt.% dispersed phase droplets in an 8 cm diameter vessel at 2000 rpm with 4 baffles.

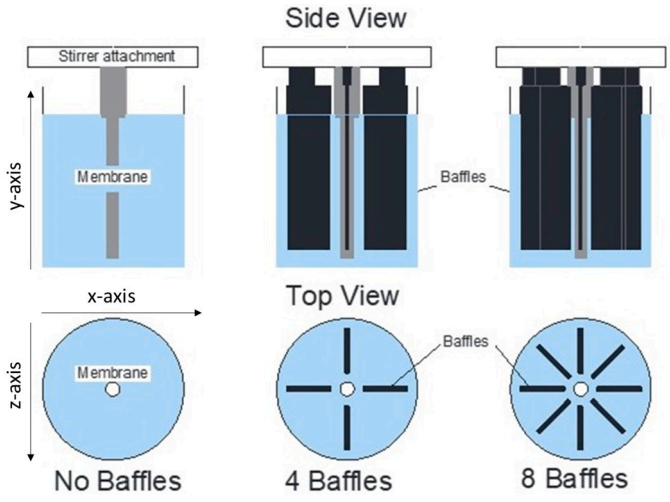

Fig. 2. Diagram of Membrane Emulsification Set-Up.

emulsifier at a concentration of 1 wt.% was added to the process vessel solution to mimic as much as possible the continuous phase used in flux experiments and to ensure the (tracer) particle surface would be adequately covered, as tests performed in the absence of the surfactant caused the particle to remain entrained at the surface of the fluid. In addition, it was desired to evaluate the validity of the PEPT results considering no dispersed phase droplets were present in the above-described process fluids. This was carried out by comparing the PEPT results obtained for the vessel with no dispersed phase. Fig. 1 shows the difference in spatial velocity distributions obtained for process fluids with and without the presence of dispersed phase droplets at a concentration of 10 wt.%. This exemplifies the little difference in the data obtained, both in terms of streamline patterns and absolute velocities. In general, these small differences were consistent for other forms of PEPT results (granular temperature, dispersion data, etc.), hence only PEPT results with pure glycerol/water systems are shown hereafter. A tracer of estimated density 1100 to 1200 $kg\ m^{-3}$, approximate diameter 290 μm, and 0.95 sphericity, was used to map the hydrodynamic conditions inside the process vessel. The particle had a calculated maximum Stokes number of 0.03, and hence is considered to have low enough inertia to closely follow fluid streamlines (Pérez-Mohedano et al., 2015).

2.2. Methods

2.2.1. Investigation of emulsion throughput

Flux experiments were performed using a tubular laser-drilled stainless-steel membrane of approximate pore diameter of 25 μm (Laser Micromachining Limited, UK), of 10 mm in diameter and 60 mm in length. The membrane was mounted on an IKA Eurostar digital overhead stirrer and positioned in the process vessel. The process vessel was interchangeable, where those employed in this study were two beakers of approximately 10 and 8 cm internal diameter, corresponding to investigated membrane surface shear rates of 1.06 to 4.23 s^{-1} and 1.66 to 6.65 s^{-1} respectively. The batch sizes used were therefore modified between 300 to 500 g to ensure complete immersion of the membrane in the process fluid. The process fluid employed in this case consisted of distilled water with the desired quantity of emulsifier dissolved/dispersed within, as specified in section 2.1.1. A diagram of the described set up is given in Fig. 2. The variation of the dispersed phase flux through the membrane was investigated at three different TMPs, baffle configurations, and rotational speeds, as specified in Table 1. The variation of the dispersed phase added with time was measured using an Ohaus Pioneer Plus Precision model scale, where the added mass was recorded for time steps of 10 seconds until 10 wt.% oil was reached.

2.2.2. Measurement of droplet size and droplet size distributions

Emulsions resulting from the flux experiments described above were characterised in terms of droplet size and droplet size distribution (DSD) using either static multiangle light scattering (SMLS), performed in a Malvern Mastersizer 2000 (Malvern Instruments, UK), or Image Analysis and Processing techniques using images obtained from a light microscope (Leica DM 2500 LED). The droplet size measurements were carried out at the earliest opportunity (within 10 - 20 minutes of the end of the RME process), where in the case of the measurements using the laser diffraction technique, the Mastersizer equipped with a Hydro SM manual small volume sample dispersion unit was used to disperse the droplets to avoid multiple light scattering and were measured in triplicate, whilst for the light microscope, droplets were sampled from the emulsion using a 5 ml serological pipette and placed on a slider to be analysed through image processing techniques. All experimental data sets exhibited approximately monomodal normal distributions, as demonstrated by Fig. 3. Hence the respective characterisation of droplet size and DSD involved evaluation of the volume mean diameter, D_{43} (Equation (1)), and the span (Equation (2)) to represent the width of the volume weighted distribution:

$$D_{43} = \frac{\sum D_i^4 n_i}{\sum D_i^3 n_i} \tag{1}$$

$$Span = \frac{D_{90} - D_{10}}{D_{50}} \tag{2}$$

where n_i and D_i are respectively the number of droplets within a certain size class and the corresponding mean diameter of that size class, and D_{10}, D_{50}, and D_{90} are the droplet diameters below which 10, 50 and 90% of the total dispersed phase volume resides in the distribution.

2.2.3. PEPT experiments

Preparation of aqueous phase: The process vessel fluid was prepared by combining the required amount of Tween 20, water, and glycerol. The solutions were then mixed for 3-5 minutes using a magnetic stirrer to homogenize the process fluid, as both Tween 20 and Glycerol are highly miscible in water (Wexler, 2014).

Preparation of radioactive tracer: The particle tracer employed in this study was an anion exchange resin (Dowex, Sigma-Aldrich), radioactively labelled using ^{18}F, with approximate half life of 109 minutes (Parker and Fan, 2008). The ion resin was indirectly activated via im-

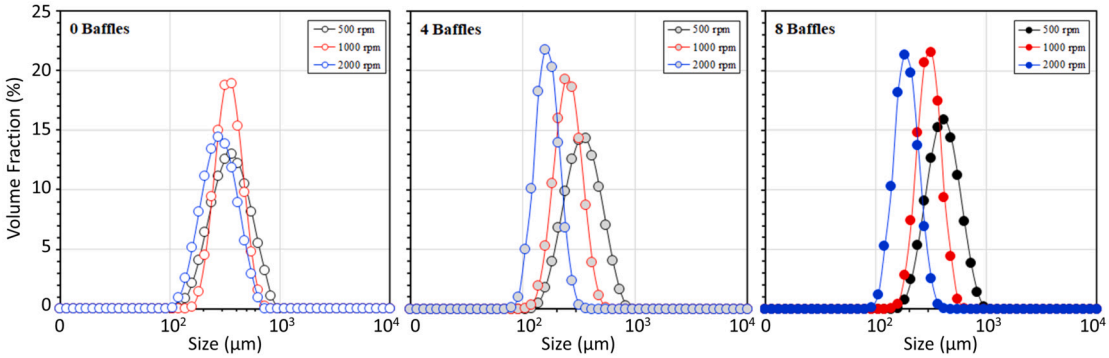

Fig. 3. Selected Examples of Droplet Size Distributions for all Experimental Conditions and Baffle Configurations.

mersion in fluorine-18 ion rich ultrapure water, which itself was formed in an MC40 Cyclotron through helium-3 bombardment.

PEPT experimental procedure: PEPT experiments were performed at a rotational speed of 2000 rpm with three different baffle configurations, as specified in Table 1 and Fig. 2. The trials were carried out at the Positron Imaging Centre at the University of Birmingham (United Kingdom), employing an ADAC Forte dual-headed positron camera with quantum efficiency of approximately 23% for detecting 511 keV photons (Parker et al., 2022).

As aforementioned, three different baffle configurations were investigated in two different size process vessels with two correspondingly different baffle dimensions and batch sizes, such that baffles were not touching the bottom or sides of the process vessel and the liquid level height was sufficient to completely submerge the membrane. All experiments employed the same particle tracer. The process vessel was placed between the two cameras at a head separation of approximately 500.22 mm with the process vessel fluid height being approximately 160 to 230 mm above the bottom of the camera edge, as depicted in Fig. 4. Experiments were allowed to run for at least 1 and up to 2 hours, depending on the membrane rotational speed and activity of the particle tracer, to guarantee sufficient occupation of the tracer in each section of the process vessel, such that good resolution in each data set could be obtained. Pre-processing of the resultant data was performed using the PEPT-ML algorithm (Nicuşan and Windows-Yule, 2020), since this performs strongest in terms of delivering the best combined spatio-temporal resolution for experiments employing single particle tracers (Windows-Yule et al., 2022b). Post-processing of the PEPT data involved calculation of velocity components throughout the experiment, the details of which are given in Appendix A.

Initially, it was desired to run PEPT experiments at three different membrane rotational speeds at three different baffle configurations (Table 1), implying 9 different set-ups for each size of process vessel. However, the spatial velocity data obtained in the 4 baffle configuration for speeds of 500 and 1000 rpm were insufficient to adequately map the flow conditions inside the vessel. This is likely due to stagnant zones introduced near the bottom and corners of the vessel when using baffles. Hence, the following analysis details only the results of data obtained for a rotational speed of 2000 rpm.

It was also originally envisioned to conduct all experiments using only water and Tween 20 emulsifier as the process vessel fluid. However, due to a small density difference between the particle and process fluid, the particle was insufficiently suspended in the vessel to accurately model flow conditions when pure water was employed. The particle was in fact observed to become lodged at the bottom of the vessel for extensive periods with and without baffles. Incrementally increasing the fluid density using glycerol allowed the particle to become neutrally buoyant, where a 70 wt.% glycerol concentration delivered the fewest blank cells in spatial velocity data, indicating that the particle was sufficiently buoyant to occupy most regions of the vessel and

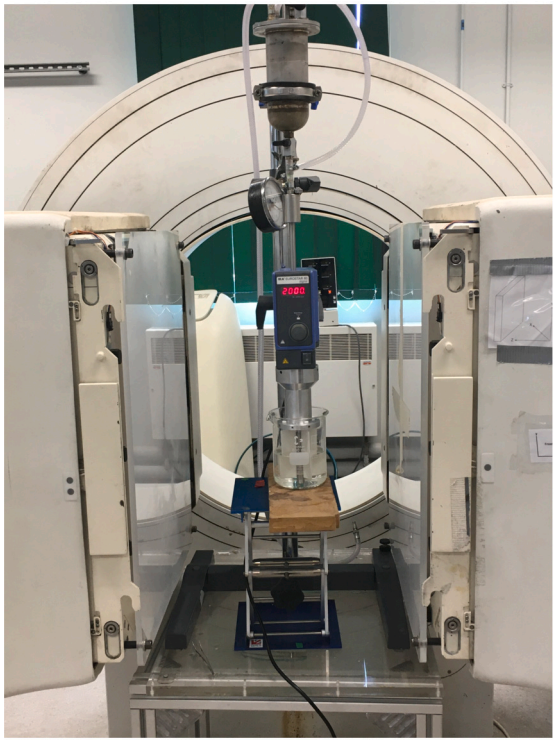

Fig. 4. Setup employed for PEPT experiments.

mimic fluid behaviour. Glycerol was chosen as it is a Newtonian fluid over the investigated range of shear rates, whilst also having been previously used in other RME studies (Lloyd et al., 2014).

3. Theoretical background

Many previous studies have outlined the importance of considering both the dispersed and continuous phase fluid flow behaviour in rotating membrane emulsification (RME) (Spyropoulos et al., 2014b; Lloyd et al., 2014; Arkoumanis, 2019; Lloyd, 2016; Peng and Williams, 1998; Schröder et al., 1998; Vladisavljević and Williams, 2005). Although most authors consider the effects of both on emulsion microstructure, many seem to neglect the effect of the latter on achievable emulsion production rates, and assume a constant throughput rate over time, as predicted by the Darcy equation (section 4.1). It is well documented in membrane filtration studies that crowding of solute at the membrane surface can affect permeate flux considerably, hence manipulation of the hydrodynamic conditions in these units to enhance surface shear and turbulence-inducing Taylor vortices is commonplace (Jaffrin, 2012; Pinilla et al., 2020; Serra et al., 1999). This includes rotation of cylindrical membranes whilst the permeate is pushed through, so as to exploit

the phenomenon of increased Talyor vortices in the annular gap, in some cases achieving a flux of up to 5.75x10$^{-5}m^2m^{-2}s^{-1}$ for a rotational speed of 3,600 rpm. Hence it is possible that the hydrodynamic factors that are relevant to membrane filtration may also hold significance for the RME technique.

The theory behind the formation of Taylor vortices stems from consideration of the flow conditions for a Newtonian fluid situated between two concentric cylinders; the inner one rotating and the outer one remaining stationary. The hydrodynamic behaviour in this case can be described by two dimensionless numbers; the Reynolds number, Re, and the Taylor number, Ta, defined as follows:

$$Re = \frac{\omega R_1 (R_2 - R_1)\rho_c}{\mu_c} \tag{3}$$

$$Ta = Re\sqrt{\frac{2(R_2 - R_1)}{R_1 + R_2}} \tag{4}$$

where ω is the angular velocity of the rotating membrane, R_1 and R_2 are the respective radii of the outer membrane surface and inner vessel wall, ρ_c is the density of the continuous phase fluid, and μ_c is the continuous phase viscosity (Aryanti and Williams, 2018). Below a certain value of Ta, simple laminar shear flow exists between the cylinders. Beyond this value, the flow becomes unstable and secondary flows known as Taylor vortices develop. A further transition exists at yet higher Ta values, beyond which the flow becomes turbulent (Bird, 1994; Vanyo, 2001). In the case of RME, the relevant critical Ta values are 41.3 and 800, between which the flow is laminar with vortices (Ekanem et al., 2022), and which is said to be the ideal region for droplet formation due to the increased shear applied to forming droplets via the action of rotating Taylor vortices (Lloyd, 2016).

Equation (3) demonstrates not only the importance of the vessel dimensions on dynamic fluid conditions, but also the effect of the continuous phase properties. Previous works (Ekanem et al., 2022; Vladisavljević and Williams, 2006) seemingly assume that, because of the relatively low dispersed phase volume, typically from 1 - 10%, the continuous phase viscosity near the membrane surface remains constant throughout the incorporation of dispersed phase droplets, implying good mixing throughout the annular gap. However, if conditions in the vessel are highly laminar and conducive to vortex formation with no crossover of streamlines in the radial direction, the lighter (lower density) dispersed phase droplets are likely to congregate near the membrane surface and thus significantly increase the local effective viscosity (Guo et al., 2014; Coulson et al., 1999). An increased local effective viscosity caused by a high dispersed phase emulsion formed due to congregation of droplets could thus further decrease turbulence near the membrane surface, whilst also hindering the transport of emulsifier to newly-formed droplet interfaces. These factors would affect, respectively, the droplet detachment time, t_d, and the droplet growth volume, V_g, i.e. the volume contribution to the droplet before the applied shear is sufficient to detach the droplet (Peng and Williams, 1998), which are said to be directly related to the volumetric flow rate through a singular pore channel, q_d:

$$q_d = \frac{V_f - V_g}{t_d} \tag{5}$$

where V_f is the final droplet volume (Lloyd et al., 2014). Hence equation (5) shows that if both t_d and V_g increase, the overall flux will be reduced. The crowding of droplets near the membrane pores could also have a steric effect, hindering new droplet detachment from the surface, having a directly opposite affect to the “push off” force said to aid detachment, as described in previous works (Spyropoulos et al., 2014b). Finally, an increased growth volume would likely also lead to an increase in final droplet size, which may be further exacerbated by excessive droplet coalescence after detachment due to the high population of droplets near the membrane. Hence, emulsion droplet size and monodispersity would be adversely affected by the described phenomena.

It is thus evident that a new approach is needed to remedy the poor flow conditions encountered in RME equipment. Baffles are commonly used in industrial applications to prevent swirling and vortexing in mixing equipment, effectively destroying circular flows whilst enhancing the mixing rate (Vogel and Todaro, 2014; Youcef et al., 2017). It is thus proposed that the addition of baffles in the process vessel and near the membrane surface will aid to disrupt circular trajectories followed by fluid streamlines, introducing a level of re-circulation in the continuous phase. To evaluate the effectiveness of this strategy, and to gain further understanding of the hydrodynamic conditions present in RME unit equipment, flux experiments have been performed with the methodology described in section 2.2.1, supported by a PEPT study to allow visualisation of fluid streamlines, velocity distributions, and granular temperature profiles.

4. Results and discussion

4.1. Effect of baffle configuration on dispersed phase transmembrane flux

Fig. 5 shows the variation of dispersed phase throughput over time for different baffle configurations at 1, 1.5, and 2 bar transmembrane pressures (TMPs) and 2000 rpm membrane rotational speed, whilst Fig. 6 shows the average total flux, J_d, for various experimental conditions, calculated as follows:

$$J_d = \frac{M_d}{\rho_d A_m t_p} \tag{6}$$

where, M_d is the total mass of dispersed phase added, ρ_d is the dispersed phase viscosity, A_m is the total membrane surface area, and t_p is the total processing time required to reach M_d (Lloyd et al., 2014). The transmembrane flux, J_d is related to the TMP, ΔP_{TM}, through Darcy’s law:

$$J_d = -\frac{K\Delta P_{TM}}{\mu_d L_p} \tag{7}$$

where K is the membrane permeability and L_p is the pore channel length (Spyropoulos et al., 2014b). In general, Fig. 6 demonstrates good experimental adherence to the predicted increase in flux with TMP, with each baffle configuration showing a linear fit with an R-squared value > 0.9 for all baffle configurations and for both emulsifiers. Table 2 shows the values of fitting parameters obtained when both linear and power law models were fit to the data in Fig. 6. Power law models were fit as the exponents of such models can give a sense of the departure from the Darcy equation with operating time, as suggested by Lloyd et al. (2015). Notably, the slope of the linear fit remains relatively constant between treatments for the measurements with T20 emulsifier, with an average calculated permeability constant of 6.98x10^{-14} m^2 +/- 2.05x10^{-14} m^2 (calculated using equation (7)), where, according to the linear model, the increase in flux between baffle configurations is mainly attributed to an increase in the y-intercept. In addition, the increase in y-intercept brings the data closer to the expected trend according to equation (7), where zero TMP should give zero flux through the membrane. Conversely, the calculated permeability obtained from the linear fit parameters in Table 2 varies with the measurements using silica emulsifiers from 5.91 to 7.99x10^{-14} $m^2\ s^2\ kg^{-1}$, corresponding to an average 19.2% increase in permeability from 0 to 8 baffles. These differences in fitted values suggest that, for the T20 emulsifier, the inclusion of baffles causes a defined increase in flux across all measured TMPs, whereas for silica particles, the increase in flux can be attributed to an apparent increase in membrane permeability. The latter observation may stem from a steric hindrance effect when no baffles are employed and droplets are allowed to congregate near the membrane, which is prevented when employing baffles. This effect would be more important for the high surface tension silica stabilised emulsions, as without this hindrance a “push off” force is allowed to prevail (Spyropoulos et al., 2014b), increasing the perceived membrane permeability with baffling.

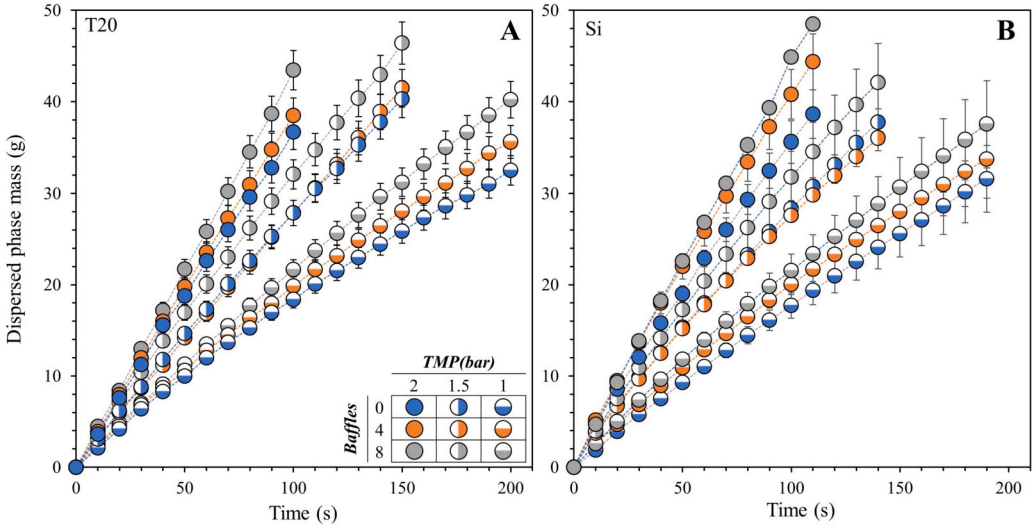

Fig. 5. Mass throughput vs time data for 10 wt.% o/w emulsions stabilized by A) 1 wt.% Tween 20 (T20) and B) 3 wt.% colloidal silica (Si).

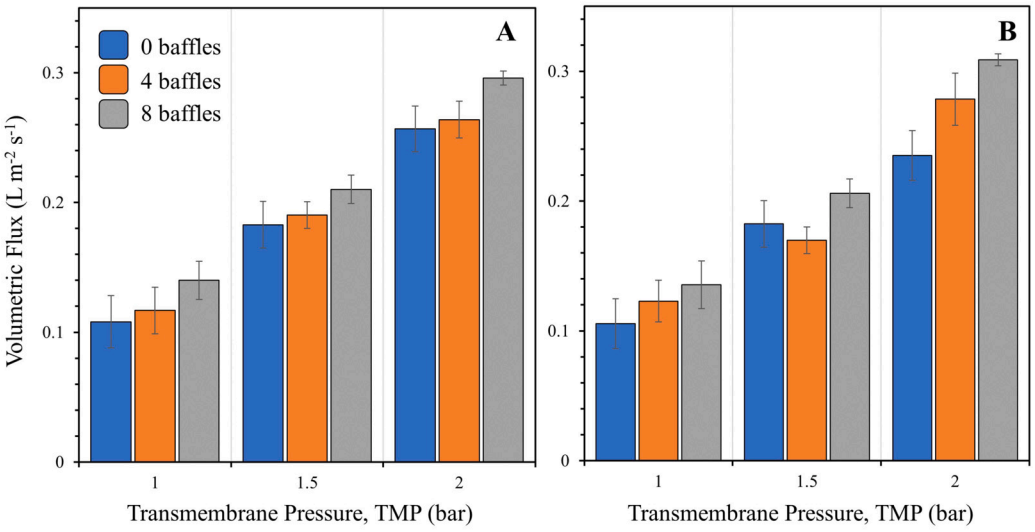

Fig. 6. Average transmembrane flux ($Lm^{-2}min^{-1}$) at different pressures and baffle configurations for 10 wt.% o/w emulsions stabilized by A) 1 wt.% Tween 20 and B) 3 wt.% colloidal silica with a membrane rotation rate of 2000 rpm.

Table 2
Values of Parameters for Linear and Power Law Models Fit to Averaged Flux Data ($m^3\,m^{-2}\,s^{-1}$).

Tween 20 Emulsifier						
Configuration	Linear fit	Linear fit	R-Squared	Power law	Power law	R-Squared
Baffles	a ($m^2\,s\,kg^{-1}$)	b ($m^3\,m^{-2}\,s^{-1}$)	R^2	a ($m^2\,s\,kg^{-1}$)	b ($m^3\,m^{-2}\,s^{-1}$)	R^2
0	1.50E-09	-4.23E-05	0.999	5.00E-11	1.26	0.9995
4	1.47E-09	-3.03E-05	0.999	1.19E-10	1.18	0.9997
8	1.56E-09	-1.84E-05	0.9966	6.00E-10	1.07	0.9974
Silica Emulsifier						
Configuration	Linear fit	Linear fit	R-Squared	Power law	Power law	R-Squared
Baffles	a ($m^2\,s\,kg^{-1}$)	b ($m^3\,m^{-2}\,s^{-1}$)	R^2	a ($m^2\,s\,kg^{-1}$)	b ($m^3\,m^{-2}\,s^{-1}$)	R^2
0	1.29E-09	-2.00E-05	0.9884	1.56E-10	1.17	0.9846
4	1.56E-09	-4.30E-05	0.95	2E-10	1.15	0.9564
8	1.73E-09	-4.31E-05	0.9884	2E-10	1.13	0.9918

To further investigate these trends and their adherence to the Darcy equation (equation (7)), the data can be fit to a power law model. According to equation (7), the flux should be directly proportional to the TMP with an exponent of 1, especially at such high values. However, for both types of emulsifier, the unbaffled configuration gives an exponent >1, which approaches unity upon inclusion of baffles, demonstrating how the baffled vessel reduces the time dependency of the measured flux.

The variation in flux for different configurations is further emphasized when regarding Fig. 5, where the throughput for unbaffled experiments is shown to decrease with processing time and in general is lower than those for experiments with baffles. As previously explained (sec-

tion 3), this could be attributed to the accumulation of droplets near the membrane surface due to the poor mixing environment and vortexing, increasing the local continuous phase viscosity and hence also the droplet detachment time and growth volume. The deviation from theoretical predictions, as well as overall increase in flux upon the inclusion of baffles, suggests the need to incorporate an additional parameter in the Darcy equation (equation (7)), accounting for the varying hydrodynamic conditions in the process vessel for membrane emulsification.

A further notable trend is the greater flux enhancement seen when using 8 rather than 4 baffles, resulting in a 14.2% and 14.1% average increase in flux for Tween 20 and silica emulsifiers respectively as compared to the unbaffled configuration across all TMPs. This could be explained by considering the fluid motion in close proximity to the rotating membrane surface. In the baffled configuration, the flow near the membrane is more restricted as compared to the unbaffled configuration due to the presence of baffle edges. These restrictions likely cause a pressure drop (Stewart and Arnold, 2009), increasing the TMP difference near the membrane surface, thus encouraging dispersed phase throughput according to equation (7). Therefore, the addition of more baffles would further augment flow resistance and pressure drop, leading to the observed elevation in flux for 8 as compared to 4 baffles. This theory also corresponds well with the aforementioned variation in y-intercept for the fitted linear equations. Furthermore, more resistance may increase the viscous drag force, F_D, and dynamic lift force, F_L, due to a higher drag coefficient, C_d, and wall shear, τ_w, respectively, according to equations (8), (9) and (10):

$$F_D = 6\pi C_d R_d \mu_c v_{rel} \tag{8}$$

$$F_L = k_l \frac{\tau_w^{1.5} D_d^3 \sqrt{\rho_c}}{\mu_c} \tag{9}$$

$$\tau_w = \mu_c \frac{\pi R_1^2 N}{15(R_2^2 - R_1^2)} \tag{10}$$

where R_d is the droplet radius, v_{rel} is the relative velocity between the continuous phase fluid and the membrane, k_l is the lift coefficient, D_d is the droplet diameter, and N is the rotational speed (Lloyd et al., 2014; Egidi et al., 2008). An increased drag and lift force has been shown through previous studies and force/torque balances to decrease the droplet growth volume (Spyropoulos et al., 2014b; Arkoumanis, 2019; Lloyd, 2016), thus improving the transmembrane flux. However, the discussion in section 4.2 shows that there is little difference observed in droplet size for 4 and 8 baffles, hence it is possible that the latter effect varies little between the baffled configurations, whereas the former pressure drop effects are mostly responsible for the observed differences.

4.2. Effect of baffle configuration on emulsion droplet diameter and monodispersity

One of the key advantages of Membrane Emulsification (ME) is commonly cited as the ability to produce highly monodisperse emulsions of defined size, principally limited by the membrane pore dimensions (Hancocks et al., 2016; Lloyd et al., 2015). Furthermore, RME is proposed to facilitate droplet removal from the membrane surface due to the combined effect of a centrifugal force and density difference acting between the dispersed and continuous phase (Spyropoulos et al., 2014a), aiding droplet detachment and lessening the likelihood of droplet coalescence near to the membrane surface, which in turn decreases the average droplet size and system polydispersity (Peng and Williams, 1998). It is thus essential to consider how the inclusion of baffles might affect the described advantages to ensure the flux improvement is not at the expense of the desired emulsion microstructure. Hence, it could be hypothesised that baffles would help reduce the observed droplet size, due to increased shear and lift force described in section 4.1 (equations (8) - (10)), as well as an improved mixing environment allowing earlier adsorption of emulsifier onto the droplet interface.

Fig. 7 shows the measured mean droplet sizes (D_{43}) and span values for varying experimental conditions and baffle configurations at a membrane rotational speed of 2000 rpm. Overall, the mean droplet to pore diameter ratio ranges from 6 to 12, which is within the range of values reported elsewhere (Hancocks et al., 2016; Silva et al., 2017). It is clear that for unbaffled RME, the average droplet size and span increase consistently with TMP for both surfactant and particle stabilised emulsions, with a 41.5 and 23.6% increase in mean droplet diameter between 1 - 2 bar TMP respectively, as well as a 20.7 and 14.8% increase in span. In addition, the surfactant stabilised emulsions have consistently larger average diameter droplets as compared to the Pickering emulsions for all baffled/unbaffled configurations. This contradicts the anticipated trend, as it is expected that the surfactant would be more easily adsorbed to the droplet surface and thus promote earlier detachment from the membrane, hence the obtained result might be attributed to the increased stability of droplets when stabilized by Pickering particles, reducing the possibility for coalescence throughout the emulsification process. This explanation is further validated when regarding the decrease in relative droplet size percent difference with baffles (from 33.0 to 5.11% difference between surfactant and Pickering emulsions at 2 bar), indicating that the baffles, which are theorised to be responsible for preventing droplet congregation at the membrane surface, may reduce the extent of droplet coalescence throughout the emulsification process.

For systems employing the same emulsifier, there exist several factors which contribute to the variation of droplet size with TMP. The factors which are said to have the largest impact include the relative adsorption rate dependency of the dynamic interfacial tension (Schröder et al., 1998), increased mass transfer (Peng and Williams, 1998), spontaneous droplet detachment due to increase in interfacial free energy (Spyropoulos et al., 2014b), and increased active membrane pore fraction (Vladisavljević et al., 2004). The former two factors are said to contribute to an increased droplet diameter, whilst the latter two have the opposite effect (Lloyd et al., 2014). However, due to the relatively constant active pore fraction of the stainless-steel membrane used in this study, the increase in active pore fraction with TMP is likely not a relevant factor (Lloyd, 2016). Spontaneous detachment forces are also typically greater for higher interfacial energy systems. This is due to the enhanced role of the steric “push off” effect which leads to “spontaneous transformation-based droplet formation” (Lloyd et al., 2014). Hence these forces would be more important for emulsions formed in the presence of silica particles, possibly explaining their smaller percent increase in droplet size with TMP as compared to surfactant systems. In addition, the interfacial tension of Pickering emulsions is affected little by the concentration of particles at the droplet interface (Vignati et al., 2003), hence a faster droplet detachment relative to particle adsorption time would not significantly increase the final volume of the detached droplet, but may cause increased coalescence and thus raise the measured mean droplet diameter in this manner. Nevertheless, it has previously been observed that the former two droplet size increasing factors are dominant in this TMP range for both systems, accounting for the observed trends in the data which correspond to those found in other studies (Hancocks et al., 2016; Arkoumanis et al., 2019; Lloyd et al., 2014; Arkoumanis, 2019; Lloyd et al., 2015). The increase in span with TMP for the unbaffled configurations is also to be expected given the above explanations. A higher TMP leads to a smaller droplet formation time, meaning that there is less chance of emulsifier adsorption prior to detachment. This could cause increased coalescence upon detachment, as the drops are not adequately stabilised before entering the continuous phase. This also elucidates the smaller dependence on TMP for the span of the Pickering emulsions, as at higher TMPs the rate-limiting step for particle stabilization kinetics becomes particle transport and adsorption to the interface, which can only be improved via enhanced mixing and a higher energy input to the system to overcome the adsorption energy barrier (Arkoumanis et al., 2019).

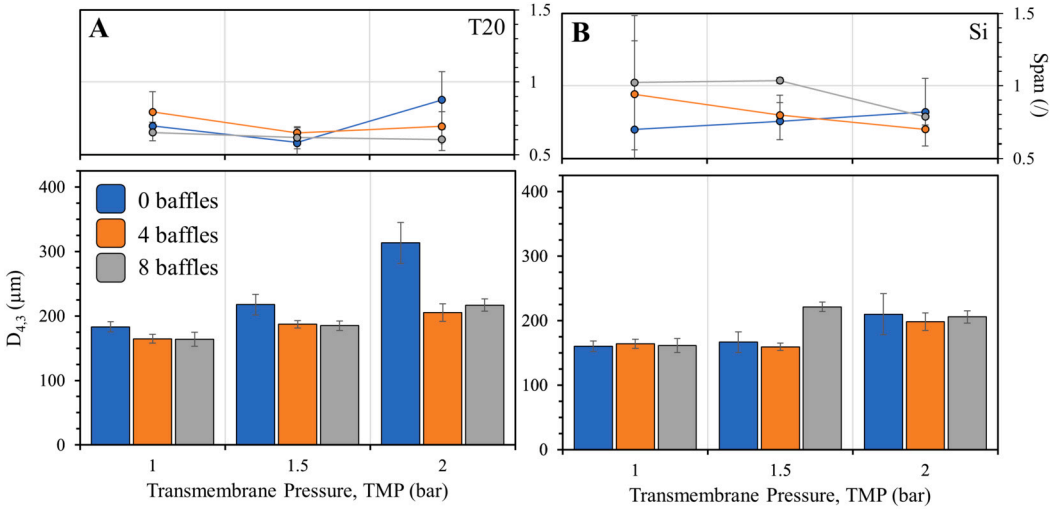

Fig. 7. Effect of baffles on the average droplet diameter and droplet size distribution span at three different transmembrane pressures for 10 wt.% o/w A) 1 wt.% surfactant stabilised emulsions (left) and B) 3 wt.% Pickering emulsions (right).

Regarding Fig. 7, it is evident that the incorporation of either 4 or 8 baffles causes a statistically significant decrease in the average drop diameter for surfactant based emulsifiers, with no significant difference between droplet sizes obtained for 4 or 8 baffles. The span values also appear to follow the opposite trend as compared to the unbaffled experiments, decreasing with TMP.

The decrease in drop diameter of surfactant systems for baffled as compared to unbaffled configurations could be attributed to an enhanced mixing environment. The rate-limiting step in surfactant-droplet stabilization kinetics is mass transfer to the droplet interface, since their adsorption is fast and largely reversible (Tripodi et al., 2020). Hence a highly dispersive environment is advantageous for such systems, as the rapid adsorption of surfactant molecules ensures a faster decrease in interfacial tension, facilitating earlier drop detachment and formation (Kalli et al., 2022), whilst also preventing coalescence once the drop is immersed in the continuous phase. In addition, if the inclusion of baffles prevents droplet congregation near the membrane surface, as has been theorised to partially explain the increase in dispersed phase flux (section 4.1), then the likelihood of droplet coalescence will decrease, thus contributing to a smaller mean droplet diameter. It is possible that once the dispersive environment is sufficiently enhanced such that surfactant diffusion is fast as compared to the droplet formation time, and droplets are effectively removed from the membrane surface, no further improvements to the hydrodynamic conditions in the continuous phase will affect the drop diameter. Hence, this would explain the little difference observed between the two baffled configurations, whilst also giving reason to the observed decreased and subsequent constant span values with TMP. Additionally, it is interesting to note the more prominent decrease in droplet size with baffles as the TMP is increased, where at 1 bar TMP the decrease is only 4%, whilst at 2 bar this reaches 46% and the droplet diameter achieves a size comparable to that at 1 bar TMP with no baffles. These results demonstrate the increased importance of more favourable hydrodynamic conditions at high dispersed phase throughput, enabling high throughput operation with baffling without significantly compromising the obtained droplet size or span.

In contrast to surfactant emulsifiers, Fig. 7 shows varying trends in the mean droplet diameter and span for Pickering particle emulsifiers, depending on the TMP. At the lowest TMP (1 bar), the mean droplet diameter between all RME setups is relatively constant, whereas the unbaffled span values are much higher for the baffled configurations. At 1.5 bar TMP, the droplet size increases for 8 baffles, and in general baffled configurations demonstrate wider spans. At 2 bar TMP, there is a relatively constant mean diameter and span for all RME configurations. Due to the widely varying data tends across different TMPs, it is difficult to determine by visual analysis whether or not baffled configurations have a statistically significant influence on droplet size and span for the Pickering emulsions. Thus, the droplet size and span data for each TMP was subjected to a one-way analysis of variance (ANOVA) test in Matlab to clarify the relative effects. A significance value of 5% was selected by convention for this preliminary study (Arkoumanis et al., 2019; Thiese et al., 2016), and the p-value results are shown in Table 3. The results show that the effect of baffles is not statistically significant ($p>0.05$) for all investigated TMPs, indicating that there is likely little impact of baffles on Pickering emulsion microstructure. Though the exact reasoning for this observation is unclear, it is suggested that this is due to a multitude of conflicting factors which tend to cancel out the overall effect.

Table 3
P-value results for ANOVA to evaluate the effect of baffles on the mean droplet size and span of silica-stabilized emulsions.

TMP	0 vs 4 baffles	4 vs 8 baffles	0 vs 8 baffles
1.5	0.886	0.350	0.343
2	0.217	0.501	0.869

The higher level of induced turbulence generated by baffled vessels aids mass transfer to the droplet surface, whilst also preventing droplet crowding near the membrane which could otherwise have inhibited particle transport. Given these considerations alone, it is expected that the baffled experiments would produce smaller droplets. However, it has been previously stated that this is not the only possible limiting factor for droplet stabilization by silica particles, especially at such high particle concentrations (Arkoumanis, 2019; Yuan et al., 2010). Particle adsorption to the interface is limited by a significant adsorption energy barrier. The rate at which a particle can overcome the energy barrier can only be increased by delivering more kinetic energy to the particle itself (Schröder et al., 2018). As is later observed in Fig. 8, the inclusion of baffles contributes to a decreased average velocity, and may even induce stagnant zones in the vessel, decreasing the kinetic energy delivered to silica particles, thus potentially slowing the adsorption rate and reducing surface coverage prior to droplet detachment, all which contributes to a larger droplet diameter. Finally, the adsorption/diffusion rate of particles relative to the droplet formation time must be considered. At low TMP, the droplets form at a slower rate, allowing more time for particles to fully cover the droplet surface before detachment, whilst at higher TMP, a faster detachment time implies a higher dependence on transport phenomena. Hence these simultaneous effects may

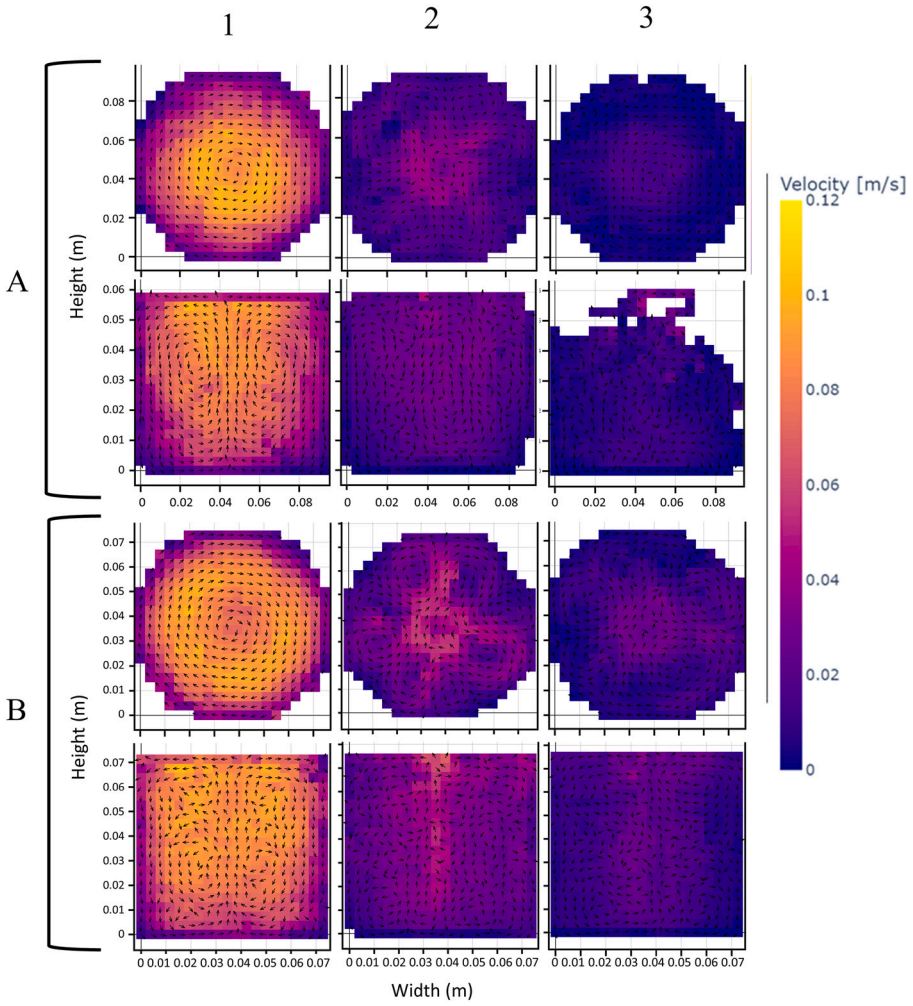

Fig. 8. Spatial velocity distributions for 70/30 wt.% glycerol/water solutions in (A) 10 cm diameter process vessel and (B) 8 cm diameter process vessel, at a membrane rotational speed of 2000 rpm for (1) 0, (2) 4, and (3) 8 baffles.

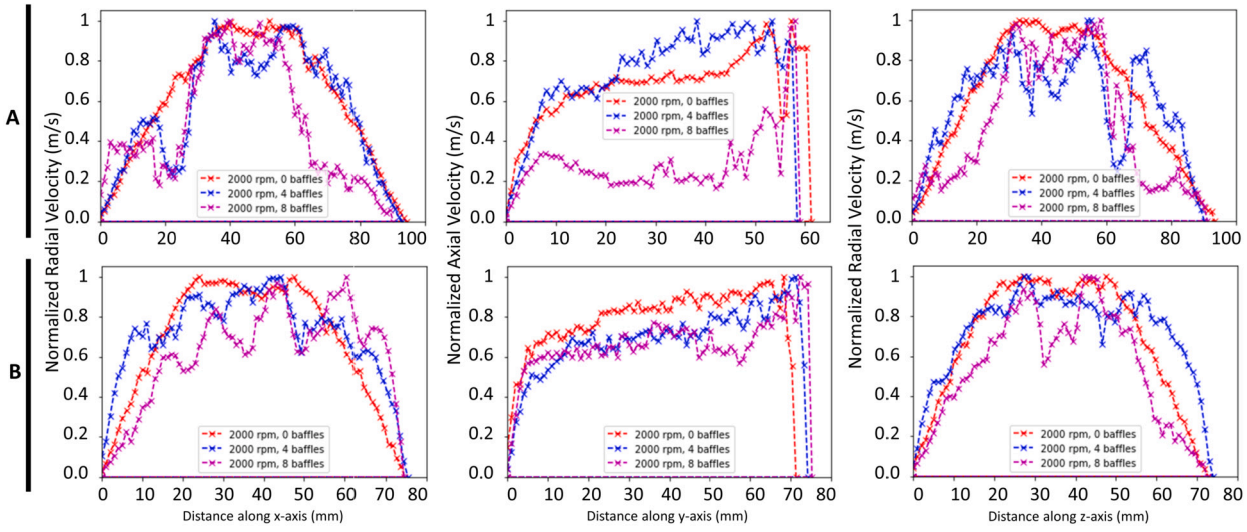

Fig. 9. Absolute normalised radial and axial velocity plots for 70/30 wt.% glycerol/water solutions in A) 10 cm and B) 8 cm diameter process vessels.

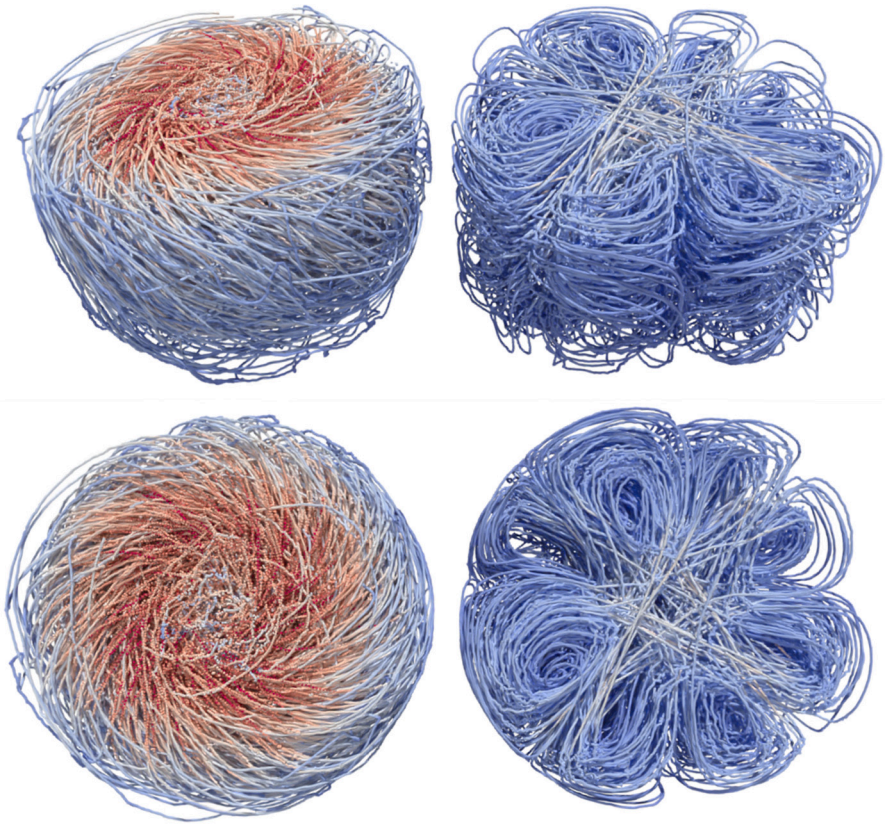

Fig. 10. Three-Dimensional visualization of fluid streamlines in the unbaffled (left) and 4-baffled (right) vessel (10 cm diameter vessel, 2000 rpm membrane rotation rate).

cancel out and thus contribute to an insignificant variation in droplet size.

4.3. Effect of baffle configuration, vessel dimensions, and continuous phase fluid properties on emulsification hydrodynamics as visualised by the PEPT technique

4.3.1. Spatial velocity distributions

Fig. 8 shows the spatial velocity distributions obtained from post-processed PEPT data for various baffle configurations and vessel sizes, whilst Fig. 9 exemplifies the difference in both radial (x and z-axis) and axial (y-axis) velocity profiles when using 0, 4, or 8 baffles. As can be expected, all figures show the highest velocity close to the membrane, and near stagnant fluid at the stationary vessel walls. A prominent feature of Figs. 8 and 9 is the difference observed in fluid flow patterns when comparing unbaffled and baffled configurations. The unbaffled configurations show a uniform decrease in linear velocity in the radial direction, as well as streamlines indicating almost perfectly circular trajectories. This is coupled with notable up-pumping axial circulation patterns in Fig. 8.1, confirming the presence of Taylor vortices in the flow, at which point Fig. 9 shows the maximum axial velocity. The latter observation is unsurprising, as all configurations have calculated Taylor numbers above the critical value required for vortex formation; however, what is unexpected is the presence of only one evident axial recirculation pattern and seemingly lower turbulence in the unbaffled vessel of larger diameter (Fig. 8.A.1) compared to multiple vortices and greater turbulence in the vessel of smaller diameter for the same rotational speed (Fig. 8.B.1), even considering that the former has a higher Taylor number (503 compared to 351). To ensure that this observation is not solely due to unsuitably low statistics, the same images at greater pixel sizes have been provided in Appendix A (Fig. 12), which confirm that the smaller vessel shows two clear recirculation patterns, as compared to the one observed for the larger vessel. This may be due to the similar order of magnitude of liquid height and annular gap, indicating that flow dynamics in this equipment cannot be solely described by the Taylor number (Childs, 2011; Ting, 2016), contrary to the assumptions implied in previous works. This could explain the difference between the observed streamline patterns for the different sized process vessels, as, if a larger annular gap is employed, there are more significant viscous losses in the fluid when travelling radially outwards, whilst the Taylor instability wavelength is also greater (Childs, 2011), requiring a taller vessel to form the same number of axial vortices as in the smaller vessel.

Fig. 8 also shows a notable difference in flow pattern for unbaffled (Fig. 8.1) and baffled (Fig. 8.(2-3)) vessels, where as predicted the baffles introduce a level of re-circulation into the flow, diverting the fast moving fluid in close proximity to the membrane outwards, thus promoting radial mixing. This is confirmed by the data presented in Fig. 9 as well as Fig. 10, which presents a comparison of the fluid streamlines in the unbaffled and 4-baffled vessel. Fig. 9 demonstrates that the velocity profile in the unbaffled vessel decreases linearly in the radial direction after a certain critical radius, whereas introducing baffles flattens this decline, whilst introducing small peaks and troughs in radial velocity away from the membrane surface as visualized in Fig. 8. Hence, though the overall velocity is significantly reduced, the presence of baffles likely aids the dispersion of emulsion droplets during flux experiments due to the break-up of circular trajectories and induced flow circulation, as visualised in Fig. 10. This is similar to the results of Mesa et al. (2021), where PEPT data showed a decrease in radial velocity around impellers upon the inclusion of a stator device, yet turbulent conditions were enhanced due to the juxtaposition of high and low radial velocity jets, creating regions of microturbulence in the investigated equipment. The breakup of fluid trajectories thus serves as a partial explanation for the significant increase in transmembrane flux, since this would decrease droplet congregation near the membrane surface resulting in the improvements described in sections 3 and 4.1.

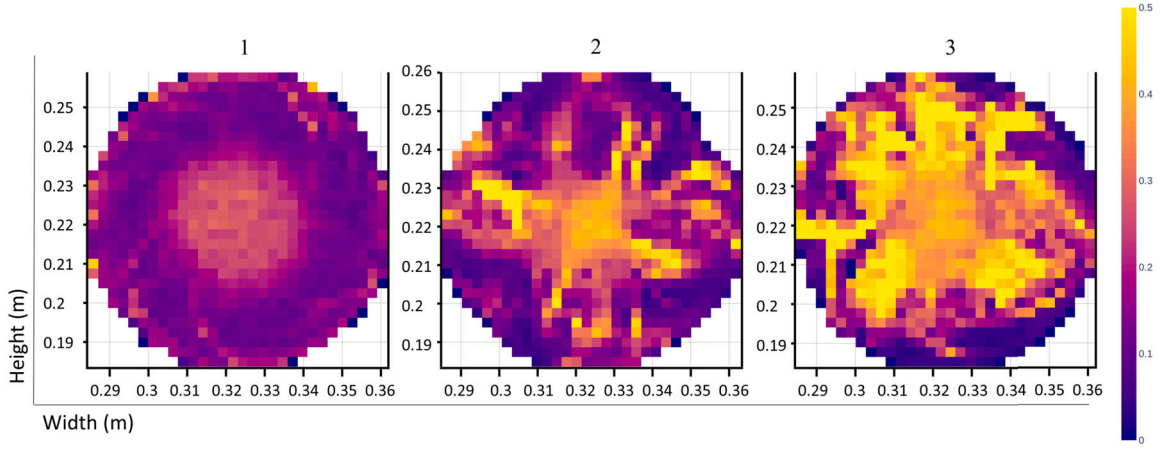

Fig. 11. (A) Granular Temperature Distribution and (B) relative standard deviation of system velocity in an 8 cm diameter process vessel for rotational speed of 2000 rpm and baffle configurations of (1) 0 baffles, (2) 4 baffles, and (3) 8 baffles.

A further marked aspect of Figs. 8-9 is the difference in average radial and axial velocity between 4 and 8 baffle configurations, as well as the general decrease in average fluid velocity near the membrane surface. The data for vessels containing 8 baffles demonstrates how the increased quantity of flow obstructions introduces an unsuitable amount of low velocity and near-stagnant zones in the vessel, resulting in the lower quality data obtained in Fig. 8.A.3, as exemplified by the white spaces in the data. This may be the cause of the negligible difference observed in terms of average droplet size data (Fig. 7). In the case of T20, though an increased amount of baffles aids in the breakup of fluid streamlines, thus improving mass transfer conditions, the low fluid velocity after the introduction of 8 baffles may hinder mass transfer of emulsifier to the forming droplet interface. This would increase the final droplet volume as well as the likelihood of droplet coalescence, as explained in section 4.1. For silica emulsifiers, the same issues would apply, however the kinetic energy of adsorption should also be taken into consideration, as a lower velocity would decrease this energy imparted to the particles and thus slow their adsorption to the droplet surface. Nonetheless, the general decrease in average velocity near the membrane surface may in fact be advantageous considering the aim to obtain higher throughputs. As explained in section 4.1, a higher drag force may contribute to an improvement in flux. The drag force is directly proportional to the relative velocity between the membrane surface and the continuous phase fluid. Considering this, the relative increase in drag can be calculated for RME configurations with 0, 4, and 8 baffles. This results in a 5.51 and 7.07% increase in drag when passing from 0 to 4 and 0 to 8 baffles respectively, which may partially explain the significant flux enhancement observed with an increased number of baffles.

4.3.2. Granular temperature distributions

To further evaluate the degree of turbulence within the system, relative standard deviations of the system velocity (RSDSV) were obtained from PEPT data. This involved calculation of local GTs (T_g) in each individual cell of defined size, in accordance with the definition of GT given by Ogawa (1978):

$$T_g = \frac{1}{D} m v^2 \tag{11}$$

where D is the dimensionality of the system, where the system under consideration was evaluated in terms of granular temperature as a 3-Dimensional case, and hence is equal to 3, and v is the fluctuation velocity obtained by taking the absolute value of the difference between the local mean flow velocity and the actual velocity in each individual cell (Windows-Yule et al., 2022b; Ogawa, 1978). Though the GT of the tracer particle cannot fully resolve small scale turbulent eddies, it gives a measure of the particle's "averaged granular fluctuating kinetic energy" (Chassagne et al., 2021), i.e. the fluctuation energy of the tracer particle at any given point in the process vessel. Hence the RSDSV, which is calculated from GT, can provide an indication of the turbulent kinetic energy distribution in the process vessel fluid. Fig. 11 shows the RSDSV profiles for several flow conditions.

Fig. 11 shows a concentration of high RSDSV nearer to the membrane in all cases. When comparing unbaffled (Fig. 11.1) to baffled (Fig. 11.3-4) vessels, a much more drastic concentration of RSDSV near the membrane and around the baffle arms can be observed, whilst exhibiting very low values in interstices between the baffles and near the vessel wall. This shows that the use of baffles further concentrates turbulence in the system near the membrane whilst also spreading it through the system, which may prevent droplet congregation in the centre region and increase shear stresses applied to detaching droplets. However, the presence of stagnant zones may be cause for concern, as these could provide the opportunity for droplet congregation and subsequent coalescence, especially if the membrane rotation rate is lower than 2000 rpm.

5. Conclusions

The present study details the first-of-its-kind application of both baffling and PEPT analysis to ME and specifically RME. Evaluation of transmembrane flux, droplet size and size distribution analysis, and corroboration of the resulting performance with differences in hydrodynamic conditions through the PEPT technique, were employed in order to investigate how the addition of baffles to process vessels affects the performance of RME operation.

In general, the baffling RME configuration was shown to significantly enhance throughput regardless of the type of emulsifier employed (either surfactant or Pickering particle species), with (on average) an 18% increase in flux from 0 (no baffles) to 8 baffles. This was attributed to a multitude of factors, including the breakup of fluid streamlines and increased turbulence. These effects were confirmed by PEPT data, in both spatial velocity distributions and granular temperature plots. Additionally, increased flow restrictions in the vicinity of the rotating membrane module are hypothesised to induce a further decrease in local fluid pressure, enhancing the transmembrane pressure (TMP) differential, whilst also allowing a (on average) 7% increase to the magnitude of the drag force.

The droplet microstructure was also shown to depend on baffle configuration, experimental/processing conditions (e.g. TMP), and emulsifier type. The largest droplet sizes across all TMPs were associated with surfactant-stabilised emulsions produced using the 0-baffle configuration. In general, surfactants showed a consistent decrease in droplet size upon the inclusion of baffles (0 vs 4 or 8), but no significant difference

between the two baffle configurations (4 vs 8). The use of Pickering particles on the other hand, resulted in emulsions of no significant differences in terms of droplet size across all configurations, which was in turn attributed to the disparity in the interfacial adsorption rates between the two emulsifier species studied. Despite the relatively modest and emulsifier-specific gains in terms of droplet size reduction delivered by the inclusion of baffles, it is extremely positive to confirm that the throughput enhancement achieved is not to the detriment of producing droplets of larger dimensions.

Overall, the results presented in the current study can have major implications for the optimisation of ME processes, and thus significantly aid in their industrial adoption. The first use of PEPT to interrogate the hydrodynamic conditions generated during ME operation also shows tremendous promise. The initial 'proof-of-principle' PEPT efforts described herein, can undoubtedly act as the foundation for future research in this area, for example in order to investigate the effect of different baffle geometries/arrangements in achieving/controlling (enhance or limit) specific hydrodynamic conditions during ME operation. Other future improvements of such techniques may also include the use of radioactive emulsion droplets in place of the particle tracer to more accurately evaluate the occupancy of the dispersed phase, as well as a more detailed investigation and quantification of how droplet congregation affects the fluid viscosity at the membrane surface in the absence of baffles.

CRediT authorship contribution statement

Chloe Huckvale Bruno: Writing – Original draft preparation, Data curation. **Ernesto Tripodi:** Data curation. **Dominik Werner:** Data curation, Data Analysis. **Christopher Windows-Yule:** Writing–review & editing, Supervision. **Fotis Spyropoulos:** Conceptualization of this study, Writing–review & editing, Supervision.

Declaration of competing interest

The authors declare the following financial interests/personal relationships which may be considered as potential competing interests: Chloe Susanna Huckvale Bruno reports financial support was provided by Royal Society of Chemistry (grant number: U21-1821928367).

Data availability

Data will be made available on request.

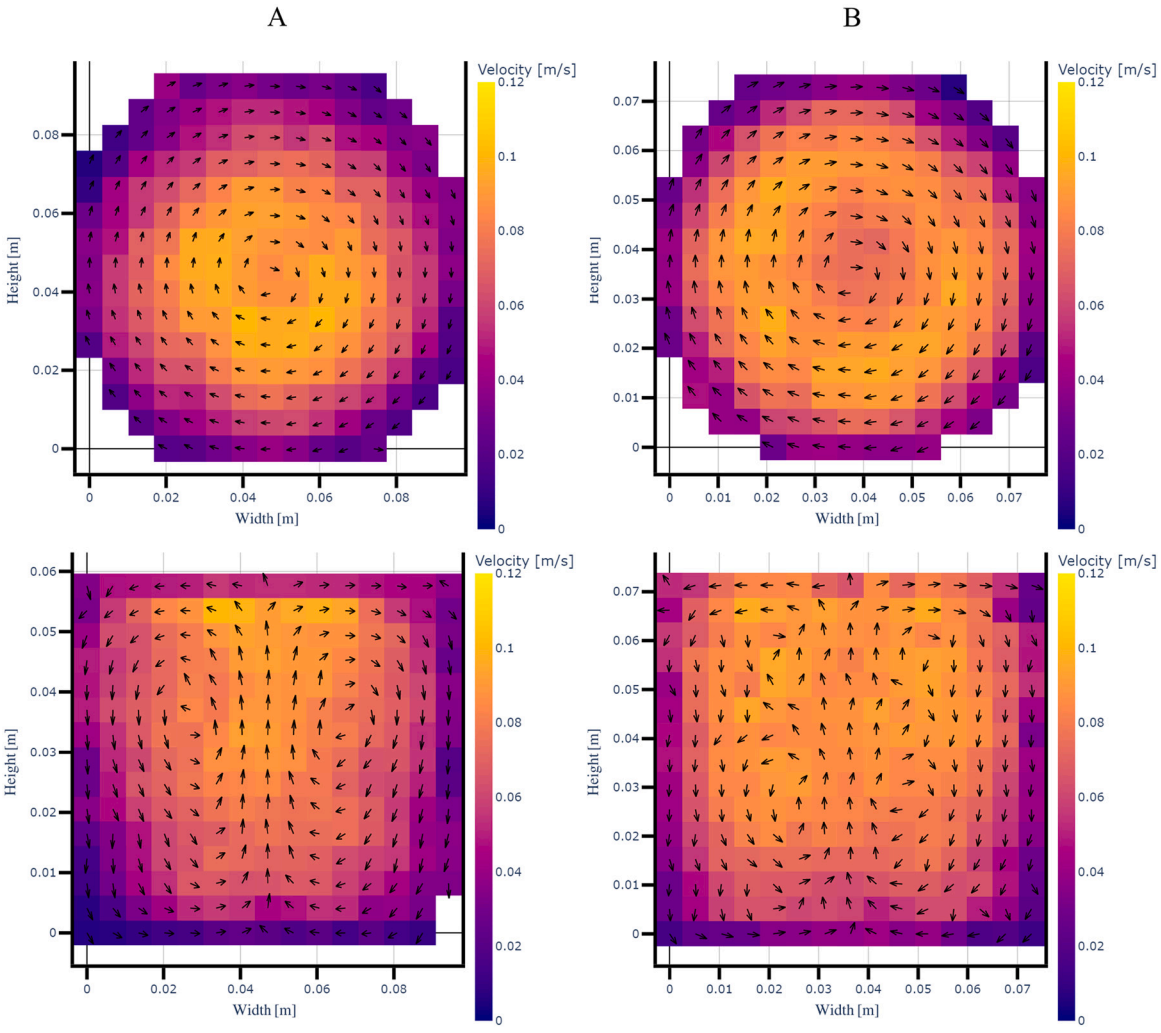

Fig. 12. Spatial velocity distributions for (A) 10 cm diameter vessel, 0 Baffles, and (B) 8 cm diameter vessel, 0 Baffles, at 2000 rpm, and 2x pixel size as compared to Fig. 8.

Appendix A. Supplementary data

A.1. Additional spatial velocity distributions

Fig. 12 shows the spatial velocity distributions of unbaffled vessels in Fig. 8 at 1.33x pixel size, demonstrating that the observations of Taylor vortices in section 4.3.1 are not solely due to unsuitably low statistics.

A.2. Calculation of velocity fields

The velocity of the tracer can be determined from the spatial and temporal data of centroids obtained from the pre-processed PEPT data. The centroid of a sample of Lines of Response (LORs) - filtered via an iterative least-squares triangulation routine - is determined within a short time interval (of the order of milliseconds). This centroid is the most likely location of the tracer particle at time t, and has coordinates in the x, y, and z dimensions. A Savitsky-Golay filter is then used to smooth the data and allow the calculation of particle velocities. The Savitsky-Golay method was used because it offers lower uncertainty in particle velocity calculations and works by fitting a polynomial to a certain number of consecutive particle positions which appear within a given time window. The derivative of this polynomial thus provides the calculated particle velocity. This computation is performed on the particles falling within a moving time window until all the particle velocities over the time of the experiment have been obtained. A more in-depth explanation of these methods is given by Van der Merwe and Leadbeater (2021).

A.3. Microscopy techniques for evaluation of emulsion microstructure

Images obtained from a light microscope of the dispersed phase droplets were analysed using image analysis techniques in Matlab. At least 10 images of different droplet collections were taken over the course of the three flux experiments to obtain at least 1000 total readings per treatment. These images were then processed using a Matlab script and function file. The script combined the results from several images of the same sample, whilst the function allowed measurement and counting of the droplets by converting and identifying circular regions in the image.

References

Arkoumanis, P.G., 2019. Design and Development of Rotating Membrane Emulsification for Production of Particle-stabilised Emulsions. PhD thesis. University of Birmingham.

Arkoumanis, P.G., Norton, I.T., Spyropoulos, F., 2019. Pickering particle and emulsifier co-stabilised emulsions produced via rotating membrane emulsification. Colloids Surf. A, Physicochem. Eng. Asp. 568, 481–492.

Aryanti, N., Williams, R.A., 2018. Analysis of rotating membrane emulsification performance for oil droplet production based on the Taylor vortices approach. Part. Sci. Technol. 36 (8), 913–919.

Aryanti, N., Hou, R., Williams, R.A., 2009. Performance of a rotating membrane emulsifier for production of coarse droplets. J. Membr. Sci. 326 (1), 16–25.

Bakalis, S., Cox, P.W., Russell, A.B., Parker, D.J., Fryer, P.J., 2006. Development and use of positron emitting particle tracking (PEPT) for velocity measurements in viscous fluids in pilot scale equipment. Chem. Eng. Sci. 61 (6), 1864–1877.

Bird, G.A., 1994. Molecular Gas Dynamics and the Direct Simulation of Gas Flows. Oxford University Press.

Chassagne, R., Chauchat, J., Bonamy, C., 2021. A Modified Kinetic Theory for Frictional-Collisional Bedload Transport Valid from Dense to Dilute Regime.

Childs, P.R.N., 2011. Chapter 6 - rotating cylinders, annuli, and spheres. In: Childs, P.R.N. (Ed.), Rotating Flow. Butterworth-Heinemann, Oxford, pp. 177–247.

Chiti, Fabio, Bakalis, Serafim, Bujalski, Waldemar, Barigou, Mostafa, Eaglesham, Archie, Nienow, Alvin W., 2011. Using positron emission particle tracking (PEPT) to study the turbulent flow in a baffled vessel agitated by a Rushton turbine: improving data treatment and validation. Chem. Eng. Res. Des. 89 (10), 1947–1960.

Coulson, J.M., Richardson, J.F., Backhurst, J.R., Harker, J.H., 1999. Coulson and Richardson's Chemical Engineering Volume 1 - Fluid Flow, Heat Transfer and Mass Transfer, 6th edition. Elsevier.

Egidi, E., Gasparini, G., Holdich, R.G., Vladisavljević, G.T., Kosvintsev, S.R., 2008. Membrane emulsification using membranes of regular pore spacing: droplet size and uniformity in the presence of surface shear. J. Membr. Sci. 323 (2), 414–420.

Ekanem, E.E., Wilson, A., Scott, J.L., Edler, K.J., Mattia, D., 2022. Continuous rotary membrane emulsification for the production of sustainable Pickering emulsions. Chem. Eng. Sci. 249, 117328.

Fangary, Y.S., Barigou, M., Seville, J.P.K., Parker, D.J., 2000. Fluid trajectories in a stirred vessel of non-Newtonian liquid using positron emission particle tracking. Chem. Eng. Sci. 55 (24), 5969–5979.

Fellows, P.J., 2000. Food Processing Technology - Principles and Practice, 2nd edition. Woodhead Publishing, p. 4.2.1.

Güell, C., Ferrando, M., Schroën, K., 2016. Membranes for enhanced emulsification processes. In: Innovative Food Processing Technologies. Woodhead Publishing.

Guo, B., Song, S., Ghalambor, A.R., Lin, T., 2014. Offshore Pipelines - Design, Installation, and Maintenance, 2nd edition. Elsevier.

Hancocks, R.D., Spyropoulos, F., Norton, I.T., 2016. The effects of membrane composition and morphology on the rotating membrane emulsification technique for food grade emulsions. J. Membr. Sci. 497, 29–35.

Herald, M.T., Sykes, J.A., Werner, D., Seville, J.P.K., Windows-Yule, C.R.K., 2022. DEM2GATE: combining discrete element method simulation with virtual positron emission particle tracking experiments. Powder Technol. 401, 117302.

Holdich, R., Dragosavac, M., Williams, B., Trotter, S., 2020. High throughput membrane emulsification using a single-pass annular flow crossflow membrane. AIChE J. 66 (6), e16958. https://doi.org/10.1002/aic.16958.

Jaffrin, M.Y., 2012. Hydrodynamic techniques to enhance membrane filtration. Annu. Rev. Fluid Mech. 44 (1), 77–96.

Kalli, M., Chagot, L., Angeli, P., 2022. Comparison of surfactant mass transfer with drop formation times from dynamic interfacial tension measurements in microchannels. J. Colloid Interface Sci. 605, 204–213.

Langford, Seth, Wiggins, Cody, Tenpenny, Daniel, Ruggles, Arthur, 2016. Positron emission particle tracking (PEPT) for fluid flow measurements. Nucl. Eng. Des. 302, 81–89.

Lepercq-Bost, É., Giorgi, M.-L., Isambert, A., Arnaud, C., 2008. Use of the capillary number for the prediction of droplet size in membrane emulsification. J. Membr. Sci. 314 (1), 76–89.

Lloyd, D., 2016. Mechanistic understanding of the Rotating Membrane Emulsification process towards the development of design and scale-up theory. PhD thesis. University of Birmingham.

Lloyd, D.M., Norton, I.T., Spyropoulos, F., 2014. Processing effects during rotating membrane emulsification. J. Membr. Sci. 466, 8–17.

Lloyd, D.M., Norton, I.T., Spyropoulos, F., 2015. Process optimisation of rotating membrane emulsification through the study of surfactant dispersions. J. Food Eng. 166, 316–324.

Mesa, D., Cole, K., Van Heerden, M.R., Brito-Parada, P.R., 2021. Hydrodynamic characterisation of flotation impeller designs using Positron Emission Particle Tracking (PEPT). Sep. Purif. Technol. 276, 119316.

Mihailova, Olga, Lim, Victor, McCarthy, Michael J., McCarthy, Kathryn L., Bakalis, Serafim, 2015. Laminar mixing in a SMX static mixer evaluated by positron emission particle tracking (PEPT) and magnetic resonance imaging (MRI). Chem. Eng. Sci. 137, 1014–1023.

Nakashima, T., Shimizu, M., Kukizaki, M., 1991. Membrane emulsification by microporous glass. Key Eng. Mater. 61–62, 513–516.

Nicuşan, A.L., Windows-Yule, C.R.K., 2020. Positron emission particle tracking using machine learning. Rev. Sci. Instrum. 91 (1), 013329.

Ogawa, S., 1978. Multitemperature theory of granular materials. In: Proc. of the US-Japan Seminar on Continuum Mechanical and Statistical Approaches in the Mechanics of Granular Materials.

Parker, D.J., Fan, X., 2008. Positron emission particle tracking—application and labelling techniques. Particuology 6 (1), 16–23.

Parker, D.J., Hampel, D.M., Kokalova Wheldon, T., 2022. Performance evaluation of the current Birmingham PEPT cameras. Appl. Sci. 12 (14), 6833.

Peng, S.J., Williams, R.A., 1998. Controlled production of emulsions using a crossflow membrane: Part I: droplet formation from a single pore. Chem. Eng. Res. Des. 76 (8), 894–901.

Pérez-Mohedano, R., Letzelter, N., Amador, C., VanderRoest, C.T., Bakalis, S., 2015. Positron emission particle tracking (PEPT) for the analysis of water motion in a domestic dishwasher. Chem. Eng. J. 259, 724–736.

Piacentini, E., 2015. Membrane emulsification. In: Drioli, E., Giorno, L. (Eds.), Encyclopedia of Membranes. Springer Berlin Heidelberg.

Pinilla, A., Berrio, J.C., Guerrero, E., Valdés, J.P., Becerra, D., Pico, P., Vargas, L., Madsen, S., Bentzen, T.R., Ratkovich, N., 2020. CFD modelling of the hydrodynamics in a filtration unit with rotating membranes. J. Water Process Eng. 36, 101368.

Schröder, A., Sprakel, J., Schroën, K., Spaen, J.N., Berton-Carabin, C.C., 2018. Coalescence stability of Pickering emulsions produced with lipid particles: a microfluidic study. J. Food Eng. 234.

Schröder, V., Behrend, O., Schubert, H., 1998. Effect of dynamic interfacial tension on the emulsification process using microporous, ceramic membranes. J. Colloid Interface Sci. 202 (2), 334–340.

Serra, C.A., Wiesner, M.R., Lainé, J.M., 1999. Rotating membrane disk filters: design evaluation using computational fluid dynamics. Chem. Eng. J. 72 (1), 1–17.

Silva, P.S., Starov, V.M., Holdich, R.G., 2017. Membrane emulsification: formation of water in oil emulsions using a hydrophilic membrane. Colloids Surf. A, Physicochem. Eng. Asp. 532, 297–304.

Sindall, R.C., Dapelo, D., Leadbeater, T., Bridgeman, J., 2017. Positron emission particle tracking (PEPT): a novel approach to flow visualization in lab-scale anaerobic digesters. Flow Meas. Instrum. 54, 250–264.

Spyropoulos, F., Lloyd, D.M., Hancocks, R.D., Pawlik, A.K., 2014a. Advances in membrane emulsification. Part A: recent developments in processing aspects and microstructural design approaches. J. Sci. Food Agric. 94 (4), 613–627.

Spyropoulos, F., Lloyd, D.M., Hancocks, R.D., Pawlik, A.K., 2014b. Advances in membrane emulsification. Part B: recent developments in modelling and scale-up approaches. J. Sci. Food Agric. 94 (4), 628–638.

Stewart, M., Arnold, K., 2009. Emulsions and Oil Treating Equipment - Selection, Sizing and Troubleshooting. Elsevier.

Tan, C., McClements, D.J., 2021. Application of advanced emulsion technology in the food industry: a review and critical evaluation. Foods 10 (4), 812.

Thiese, M.S., Ronna, B., Ott, U., 2016. P value interpretations and considerations. J. Thorac. Dis. 8 (9).

Ting, D.S-K., 2016. Chapter 1 - introducing flow turbulence. In: Ting, D.S-K. (Ed.), Basics of Engineering Turbulence. Academic Press, pp. 3–18.

Tripodi, E., Lazidis, A., Norton, I.T., Spyropoulos, F., 2020. Structure development in emulsion systems. In: Handbook of Food Structure Development. The Royal Society of Chemistry, pp. 59–92. Chapter 3 Food.

Van der Merwe, R., Leadbeater, T., 2021. Enhancing PEPT: high fidelity analysis with augmented detection. In: Proc. South African Institute of Physics (SAIP21), pp. 22–30.

Vanyo, J.P., 2001. Rotating Fluids in Engineering and Science. Dover Publications.

Vignati, E., Piazza, R., Lockhart, T.P., 2003. Pickering emulsions interfacial tension, colloidal layer morphology, and trapped particle motion. Langmuir 19 (17), 6650–6656.

Vladisavljević, G.T., Williams, R.A., 2005. Recent developments in manufacturing emulsions and particulate products using membranes. Adv. Colloid Interface Sci. 113 (1), 1–20.

Vladisavljević, G.T., Williams, R.A., 2006. Manufacture of large uniform droplets using rotating membrane emulsification. J. Colloid Interface Sci. 299 (1), 396–402.

Vladisavljević, G.T., Lambrich, U., Nakajima, M., Schubert, H., 2004. Production of O/W emulsions using SPG membranes, ceramic alpha-aluminium oxide membranes, microfluidizer and a silicon microchannel plate—a comparative study. Colloids Surf. A, Physicochem. Eng. Asp. 232 (2), 199–207.

Vogel, H.C., Todaro, C.M., 2014. Fermentation and Biochemical Engineering Handbook - Principles, Process Design, and Equipment, 3rd edition. Elsevier.

Wexler, P. (Ed.), 2014. Glycerol, in Encyclopedia of Toxicology, third edition. Academic Press, Oxford, pp. 754–756.

Windows-Yule, C.R.K., Seville, J.P.K., Ingram, A., Parker, D.J., 2020. Positron emission particle tracking of granular flows. In: Annual Reviews. Annu. Rev. Chem. Biomol. Eng. 11, 367–396.

Windows-Yule, C.R.K., Herald, M.T., Nicuşan, A.L., Wiggins, C.S., Pratx, G., Manger, Sam, Odo, A.E., Leadbeater, T., Pellico, Juan, de Rosales, Rafael T.M., 2022aet al.. Recent advances in positron emission particle tracking: a comparative review. Rep. Prog. Phys. 85 (1), 016101. IOP Publishing.

Windows-Yule, K., Nicuşan, L., Herald, M.T., Manger, S., Parker, D., 2022b. Positron Emission Particle Tracking. IOP Publishing.

Youcef, K., Bouzit, M., Ameur, H., Arab, I., Hadjeb, A., 2017. Effect of the inclination of baffles on the power consumption and fluid flows in a vessel stirred by a Rushton turbine. Chin. J. Mech. Eng. 30, 1008–1016.

Yuan, Q., Aryanti, N., Gutiérrez, G., Williams, R.A., 2009. Enhancing the throughput of membrane emulsification techniques to manufacture functional particles. Ind. Eng. Chem. Res. 48 (19), 8872–8880. https://doi.org/10.1021/ie801929s.

Yuan, Q., Cayre, O.J., Manga, M., Williams, R.A., Biggs, S., 2010. Preparation of particle stabilized emulsions using membrane emulsification. Soft Matter 6 (7), 1580–1588.